A data driven methodology for upscaling remaining useful life predictions From single- to multi-stiffened composite panels

Galanopoulos, Georgios; Fytsilis, Efthimios; Yue, Nan; Broer, Agnes; Milanoski, Dimitrios; Zarouchas, Dimitrios; Loutas, Theodoros

DOI
10.1016/j.jcomc.2023.100366

Publication date
2023

Document Version
Final published version

Published in
Composites Part C: Open Access

Composites Part C: Open Access 11 (2023) 100366

Contents lists available at ScienceDirect

Composites Part C: Open Access

journal homepage: www.sciencedirect.com/journal/composites-part-c-open-access

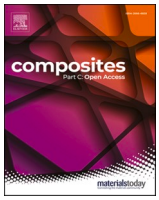

A data driven methodology for upscaling remaining useful life predictions: From single- to multi-stiffened composite panels

Georgios Galanopoulos [a], Efthimios Fytsilis [a], Nan Yue [b,c], Agnes Broer [b,c], Dimitrios Milanoski [a], Dimitrios Zarouchas [b,c], Theodoros Loutas [a,*]

[a] Applied Mechanics Laboratory, Department of Mechanical Engineering and Aeronautics, University of Patras, Rio University Campus, 26504, Rio, Greece
[b] Faculty of Aerospace Engineering, Delft University of Technology, Kluyverweg 1, 2629HS, Delft, the Netherlands
[c] Center of Excellence in Artificial Intelligence for structures, Aerospace Engineering Faculty, Delft University of Technology, the Netherlands

ARTICLE INFO

Keywords:
Structural health monitoring
Composite structures
Stiffened panels
Compression fatigue
Fiber optical sensors
Health Indicators
Remaining useful life prediction

ABSTRACT

In this paper we execute a complex test campaign to develop a novel methodology for the Remaining Useful Life (RUL) estimation of complex multi-stiffened composite aeronautical panels utilizing Machine Learning models trained with Structural Health Monitoring (SHM) data from hierarchically simpler elements, i.e., single-stiffened panels. Distributed Fiber Optical sensors (DFOS) are employed to monitor the panels' behavior undergoing variable amplitude compression-compression fatigue after multiple impacts. A data processing methodology is first applied to the DFOS data, to both alleviate the effect of the variable loading conditions on the monitored strain and ease the computational burden. In this upscaling endeavor, an advanced strain-based Health Indicator (HI) based on Genetic algorithms, created and validated on the single-stiffened panel data, is utilized as the prognostic feature for the RUL estimations of the multi-stiffened panels. The HI displays favorable characteristics in terms of monotonicity and prognosability which are highly desirable for more accurate RUL estimations. For the prognostic task, standard machine learning models are trained using the historical degradation data of the single-stiffened panels and a similarity analysis is performed to enhance the accuracy when predicting the RUL of the multi-stiffened panels. Despite the increased structural complexity of the multi-stiffened panels, we demonstrate that the RUL is able to be predicted with reasonable accuracy. The present work paves the road for upscaling and applying prognostic methodologies to more complex structures beyond simple coupons or generic elements.

1. Introduction

In the last few decades composite materials have seen an increased use in various fields of engineering with aerospace and automotive being some of the industries which are taking advantage of their unique mechanical properties. More specifically, composites are preferred over metallic materials due to their high strength-to-weight ratio and excellent corrosion resistance, which can reduce operational and maintenance costs. However, composite materials suffer from a significant disadvantage; their inhomogeneous, anisotropic nature, as well as the variety of different, interacting damage mechanisms make their degradation extremely hard to comprehend and model. In service, such materials are also subjected to multiple loading and environmental conditions which further complicates their degradation behavior. To this end, advanced monitoring technologies need to be employed to efficiently monitor them.

Structural Health Monitoring (SHM) is an emerging concept, gaining increased attention over the past couple of decades. Its main objective is to provide real-time assessment of the structure's integrity. The final level of SHM is prognostics, which is a core aspect of Condition Based Maintenance (CBM). In a CBM paradigm, maintenance is performed only when necessary, based on condition monitoring data [1], reducing downtime costs and increasing equipment availability and reliability [2]. In the epicenter of every prognostic task is the term Remaining Useful Life (RUL) prognosis [3], which involves the process of estimating the time-of-failure or the nominal end of life and plan accordingly the maintenance actions.

Structural RUL prognostics, especially for composite structures, is a

* Corresponding author at: Applied Mechanics Laboratory, Department of Mechanical Engineering and Aeronautics, University of Patras, Rio University Campus, 26504, Rio, Greece.
E-mail address: thloutas@upatras.gr (T. Loutas).

https://doi.org/10.1016/j.jcomc.2023.100366
Accepted 25 May 2023
Available online 26 May 2023

topic still at its infancy. The limited literature is revolved around two main philosophies to RUL estimation i.e. model-based and data-driven [4]. Model-based approaches rely on physical models to capture the degradation and estimate the RUL, while data-driven model use condition monitoring data to build the prediction models using machine (ML) learning and artificial intelligence (AI). Several researchers have attempted to study the task of RUL prognosis, although the vast majority of published works concern machinery and systems prognostics [5–7] whilst very few studies investigate the prognostics of composite structures. Concerning model-based approaches for RUL estimation of composites, in [8] a Bayesian filtering framework is presented, which considers multiple failure modes for the different failure mechanisms, for RUL estimation. Stiffness degradation models have also been used to predict fatigue life [9,10]. Corbetta et al. [11], proposed a particle filter model for damage prognosis in composite laminates, where the Bayesian framework proposed in [12] was extended to account for multiple damage mechanisms, and the approach was validated on data collected from tension-tension fatigue experiments on notched CFRP coupons. Through a modified Paris law, the damage could also be propagated into the future and make predictions regarding the RUL.

However, due to the lack of accurate, universally accepted models to characterize the degradation behavior of composite materials, data-driven models are commonly utilized which apparently request for historical degradation data to train algorithms or statistical models that carry out the prognostic task. Liu et al. [13] proposed a Gaussian Process model to predict the RUL of composite beams using damage indexes extracted from acoustic emission (AE) and PZT condition monitoring data. The two monitoring methodologies were compared in terms of RUL prediction results with AE slightly outperforming. The same group [14], proposed a methodology for a prognosis model of notched CFRP specimens subjected to uni-axial and bi-axial fatigue loading. The proposed RUL prediction model consisted of an online-diagnostics process, i.e., direct cross-correlation analysis, and the offline prognostics process via Gaussian process regression. Eleftheroglou et al. [15] also used strain data to predict the RUL of open-hole composite coupons. A Non-Homogeneous Hidden Semi Markov Model (NHHSMM) is used for the prediction tasks, which estimates the degradation state by employing condition monitoring data in order to predict the RUL. The same model was used for RUL prediction of open-hole specimens subjected to tension-tension fatigue using AE features and was compared with a Bayesian Neural Network (BNN) [16]. The NHHSMM was found to outperform the BNN, with more coherent predictions and converging confidence intervals. The previous methodology was extended in [17], which added an adaptive layer to the NHHSMM. More specifically, the model was tested on unseen events and was proven able to adapt and make accurate predictions of RUL by learning and updating its parameters in real-time. Xu et al. [18], monitored the degradation of composite laminates using AE. Damage sensitive AE features are discovered, and a Convolution Neural network is used to predict the RUL using the five most dominant features. It was observed that model performance was dependent on the degradation stage, and the best results were obtained during the final degradation stage. Galanopoulos et al. [19], proposed a degradation feature based on genetic algorithm optimization, which was used to predict the RUL of stiffened composite panels. Gaussian process regression and the NHHSMM were used, as the regression algorithms demonstrating the capability of estimating RUL in complex structures, since both approaches displayed good prediction performance.

A crucial factor for data-driven RUL prognostics is the quality of the degradation features. The three most sought properties are monotonicity, prognosability and trendability [20]. These degradation features are commonly referred to as Health or Damage Indicators (HIs or DIs). In this work we are referring to them as HIs to avoid confusion. These HIs are classified into two major categories as seen in the literature [21]. There are physical HIs (pHIs), which are tied to a physical property of the structure, such as strain or temperature and virtual HIs (vHIs), which are created solely to provide enhanced diagnostic/ prognostic performance and have no direct correlation to physical properties [21]. Examples of HIs can be found in the relevant literature. RMS is a common pHI in bearing applications [22,23]. In composites, axial strain is commonly used as a pHI in [15] to predict the RUL of open-hole coupons. Galanopoulos et al. [24], extracted pHIs from both strain and AE data collected from single-stiffened composite panels.

In the vHI front, Loukopoulos et al. [1] used the statistical properties Q and T^2 from PCA as vHIs to predict the RUL of reciprocating compressors. Shahid et al. [25], used a dimensionality reduction algorithm to reduce the size of the available inputs and created a vHI based on a

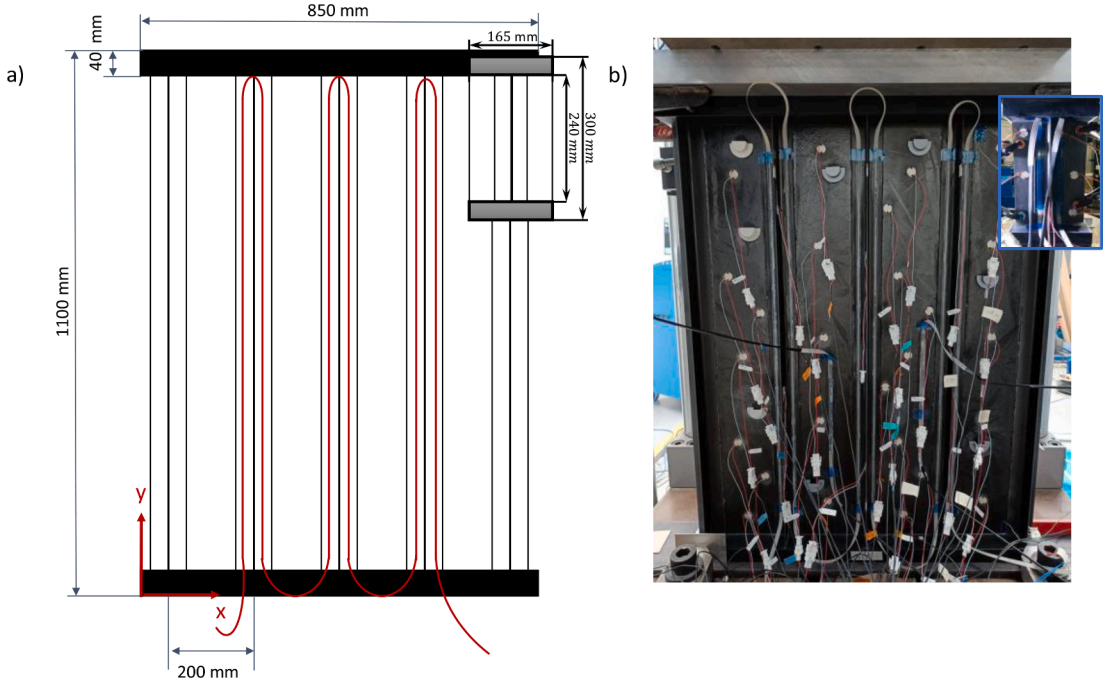

Fig. 1. Schematic representation of the MSP and sensorised MSP on the test machine.

Table 1
MSP load and damage initial damage information.

Specimen #	Impact Location X (cm)	Y (cm)	Impact Energy	Load Min.	Max.	# of Cycles to failure
MSP 01	25.3	79.5	15.2 J	19.5	195	8
				18.5	185	2076
	40	80	19.8 J	10	100	350k
				15	150	13k
	45.5	66	15.2 J	12	120	50k
				20	200	136k
	58	64.5	17.2 J	23	230	540k
						1046k
MSP 02	40.5	58	13 J	-15	-150	680k
				-17	-170	120k
				-20	-200	110k
				-23	-230	230k
						1140k
MSP 03	25.5	66.5	15.2 J	20	200	**540k**
	39.6	66.6	17.2 J			
	46	79	15.2 J			
	59.5	78.9	25.2 J			

distance metric with a radial basis normalization. Ren et al. [26] extracted time and frequency domain features which were passed through an autoencoder to automatically select and combine the most promising features. Baraldi et al. [27], utilized an Auto-Associative Kernel regression algorithm to combine together different sensor readings with respect to monotonicity, prognosability and trendability. These features corresponded to measurements from aircraft engines and the extracted hyperfeature was deemed capable of completing the RUL prediction task. In a similar notion Nguyen and Medjaher [28] used a two-stage optimization scheme to create a HI. First automated feature extraction is performed and in the second stage the extracted features fused together. Both optimization stages used monotonicity and prognosability (among others) as part of their objective functions. Genetic Algorithm was also used in [29], to combine both strain-based pHIs and vHIs into a hyperfeature for RUL prognosis of composite stiffened panels. What was shown, is that the quality of the prognostic features can greatly impact the final RUL prediction results.

From the literature review, it is evident that most research of both RUL estimation and HI formulation is not focused on composite materials or structures. The little research available is centered around simple coupons, while studies on the prognostics of more complex structures are to the best of our knowledge very limited if any. In this work we attempt to fill this gap. Building on results from our previous research [29], we investigate the feasibility of upscaling the methodologies developed for single-stiffened panels (SSPs) to multi-stiffened panels (MSPs). Strain data collected from Distributed Fiber optical sensors (DFOS) are processed in a novel way to extract useful information. The processed strains are used to calculate HIs [24] as well as an advanced HI [29], which possesses promising prognostic attributes. Finally, the advanced HI is used to predict the RUL of the SSPs using an ensemble learning framework trained with data from the SSPs and a predefined failure threshold.

The paper is structured as follows, Section 2 describes the experimental campaign and pre-processing methodologies, Section 3 presents the ensemble learning framework and the regression algorithms. Section 4 discusses the preliminary results and shows the RUL prediction, and finally, the paper is summarized in Section 5.

2. Experimental campaign

2.1. Specimen and experiment definition

Five-stringered composite panels were manufactured from IM7/8552 unidirectional prepreg CFRP by Optimal Solutions (Portugal). The layup for the skin and T-shaped stiffeners is $[45/-45/0/45/90/-45/0]_s$ and $[45/-45/0/-45/45]_s$, respectively. Resin tabs are cast on the panels' top and bottom free edges to ensure proper load introduction and uniform loading. The panels have a length of 1100*mm*and the width is 850*mm*. Distance between the stiffeners is 200*mm* and with the tabs the free length is 1020*mm*. The SSPs have a length of 300 mm and their width is 165 mm and have the exact same layup. A schematic representation of the panels' geometry is shown in Fig. 1. Before subjecting the panels to fatigue testing, a quasi-static compression test with a constant displacement rate of 0.5 mm/min is performed to assess the ultimate compression strength and guide the decision of the fatigue loads. The collapse load was estimated at 310 kN and based on this result, the initial fatigue load is determined.

To create stress concentration areas and accelerate the degradation process, Barely Visible Impact Damage (BVID) is induced. The tested panels are impacted multiple times from the skin side with various energies, using an air gun, as analyzed in Table 1. The impacts create subsurface damage in the skin-stringer interface, which will propagate under fatigue loading and ultimately lead to the failure of the panels.

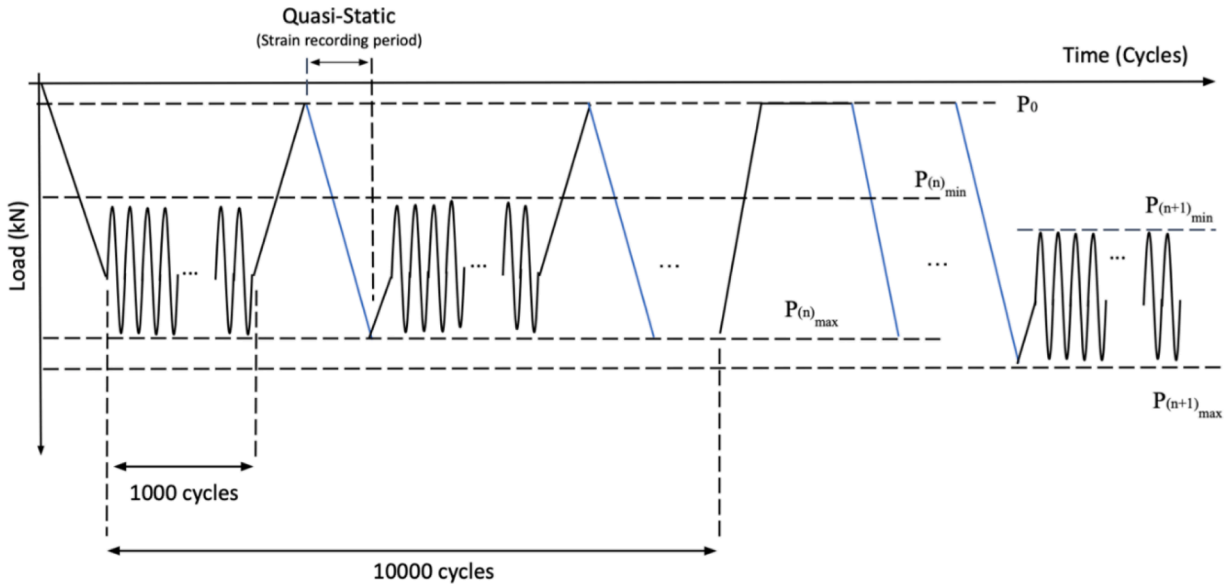

Fig. 2. Representative load sequence.

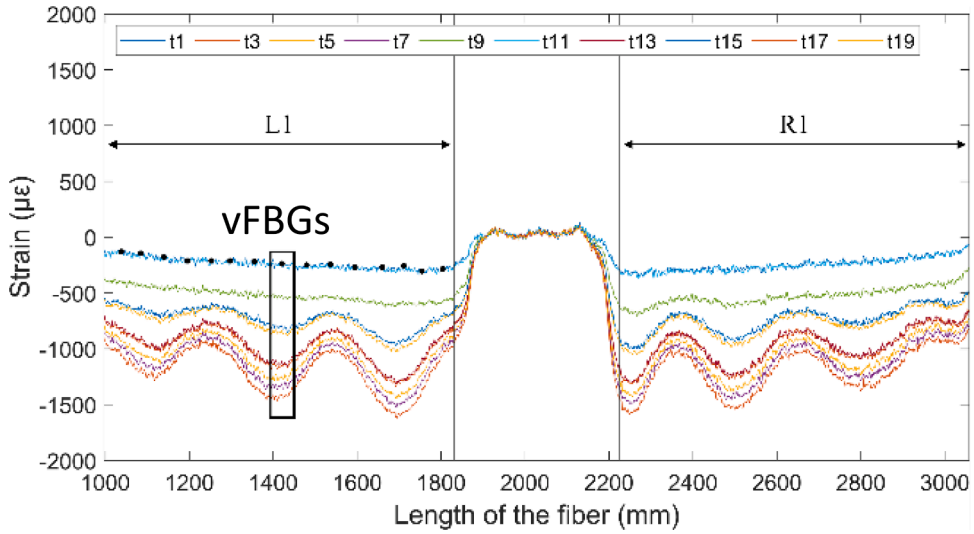

Fig. 3. Pre-processing methodology in the spatial axis.

The initial fatigue load was determined similar to [24,30], at 60% of the collapse load. The variable loading conditions are created for two reasons. First, similar to [24,29], we wanted to create different loading scenarios and evaluate the ability of our methodologies to tackle and adapt to these scenarios. Secondly, the loads were adapted in order to eliminate the snap-back behavior (buckling waves abruptly shifting to a higher mode) [31–33]. The loads and fatigue life can be seen in Table 1.

The fatigue tests are performed in the Aerospace Structures and Materials Laboratory of Delft University of Technology in an MTS hydraulic machine with 3500 kN load capacity. As mentioned earlier, variable amplitude, compression-compression fatigue tests are conducted with a constant frequency of 1Hz and load ratio of 10.

Regarding the SHM methodologies that monitor the structural integrity during the fatigue tests, the panels are equipped with a distributed fiber optic sensing (DFOS) system, as well as AE, lamb wave PZT and FBG optical sensors for vibration measurements. In this study, we utilize only strain data from the DFOS system. The DFOS is encased in a SMARTape™ [34], and is bonded with acrylic glue on both feet of the three middle stiffeners. The total measuring length is approximately 5*m*, 840*mm* per foot, focused on the middle section. The LUNA odisi-B acquisition system is used with an acquisition frequency of 23.8*Hz* and a spatial resolution of 0.65*mm*.

The loading sequence is depicted in Fig. 2. Every 1000 cycles, fatigue is stopped, and the panel is subjected to quasi-static (QS) loadings from 5 kN up to the maximum fatigue load level under a constant displacement rate of 0.5*mm/min*, during which the DFOS measurement were obtained. Every 10,000 cycles, the applied load is reduced to 5 kN to allow for LW measurements. The load is arbitrarily changed after a few tens of thousands of cycles for the aforementioned reasons.

2.2. Raw data pre-processing

Under the variable loading conditions (which are closer to real life operational conditions), the peak strains display a certain variability. This variability does not represent only damage accumulation, or structure degradation as it is desired, but also the effect of the changing loading conditions. For this reason, it is imperative to discover a pre-processing methodology attempting to eliminate the effects of the varying loads. A first attempt to eliminate the variable loading effect was proposed in [24]. In this research we build on and extend our previous methodology.

In the first step, processing is performed in the spatial domain. Since measurements are available every 0.65*mm* for 5*m*, it is evident that there is an excessively large amount of data. To reduce the amount of data, and at the same time simulate similarities to the small scale experiments of our previous research [24], where FBG point measurements are obtained, only k data points are retained per foot as virtual FBG (vFBG) sensors. Since the panels are approximately 3 time larger than the SSPs $k = 15$ was assumed since the smaller panels had 5 FBG sensors per foot. The vFBGs were spaced equally along the measurement length with a spacing of 50*mm*. An example of the strain distribution and some example vFBGs can be seen in Fig. 3. The different colored lines represent different time instances of measurement. The notations L1 and R1 correspond to the left and right foot of the first stiffener. The peaks and valleys represent the depict buckling waves captured by the fiber. The entirety of the measured strains at a specific point in the fiber (black box) are used to create the measurements of each vFBG. In Fig. 4a, the strain through time of a single vFBG is presented. Each line represents the measurements at a QS load for a representative vFBG.

On the second step, the strains are processed in the time axis, in an attempt to eliminate the load effect. n random points of the QS are sampled, equal to 1/3 of the total sample length, using a uniform distribution (see Fig. 4a zoom, where each point represents a randomly selected QS strain value) and the average of these points is considered as the strain at each time instance. The QS interval is 1000 cycles and hence each extracted strain values is assigned a timestamp of n*1000, where n is the increasing serial number of the QS. This methodology eliminates the bias of the strains towards the load since they are sampled at random unknown loads. Since the strain values are sampled randomly at each QS the resulted strains display a noisy behavior. To smooth out the effect of this noisy behavior, the final results are processed via a moving average filter (Fig. 4b).

3. Prognostic methods

An ensemble learning, similarity-based methodology is investigated for the RUL estimation of the MSP panels. Two machine learning algorithms, Gaussian Process Regression and Long Short-term Memory Networks, are trained with the SSP HI data and are employed to estimate the RUL of the MSP. This similarity ensemble learning methodology, enhances the accuracy of the predictions by looking for similarities in the degradation trends of the MSPs and SSPs. These methodologies are discussed in depth in the following subsections.

3.1. Ensemble learning

Ensemble learning entails training diverse sub-models and using their combined outputs for extrapolating the final results. A proper

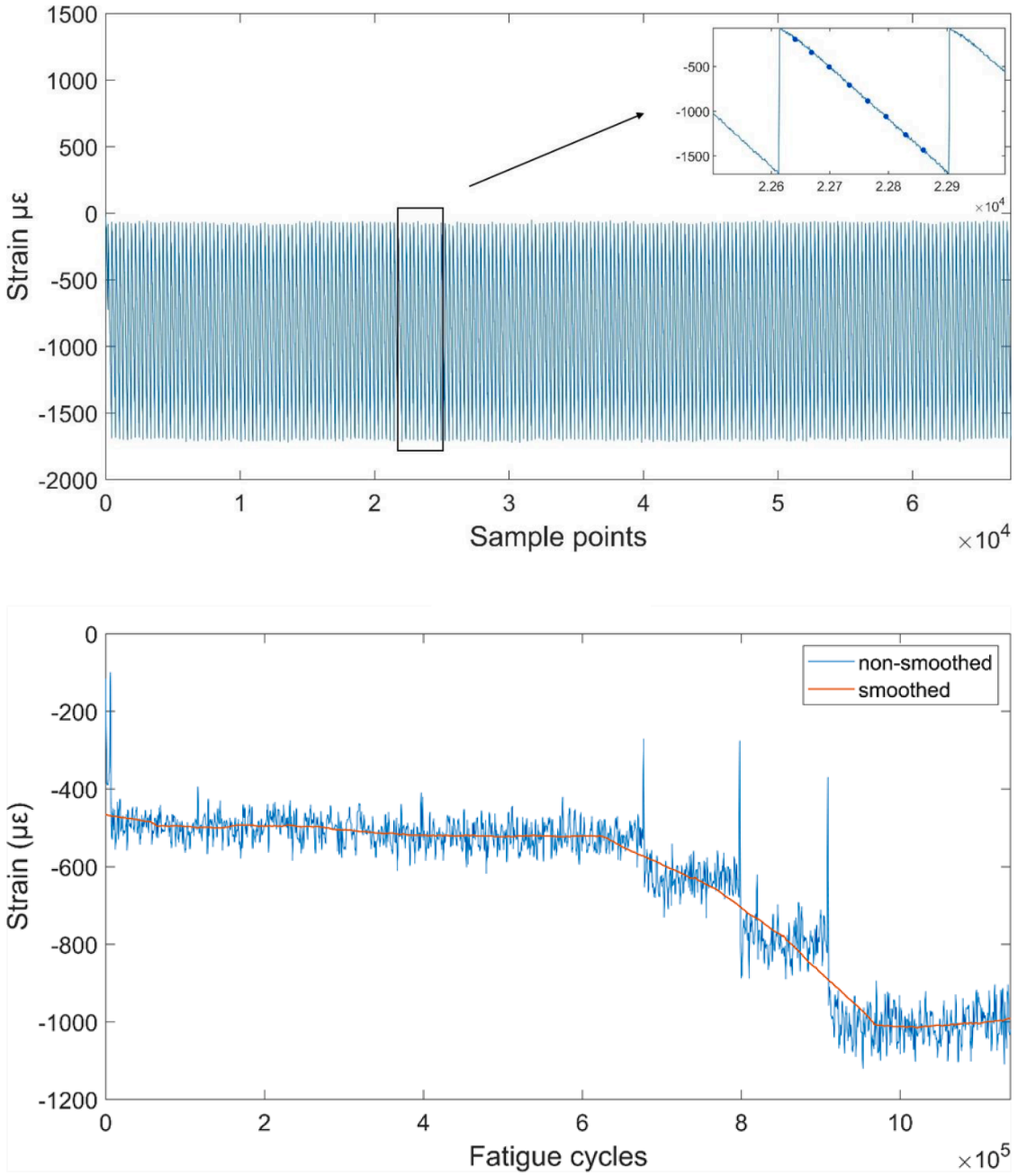

Fig. 4. Pre-processing methodology in the time axis. a) quasi-static through time for a vFBG and b) the final extracted strain.

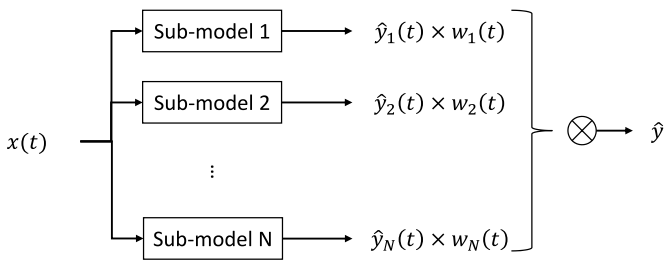

Fig. 5. Schematic representation of the ensemble learning methodology.

weighting strategy can enhance the ensemble results. Bauer et al. [35] has shown that such models are able to provide superior performance by taking advantage of the diverse outputs of each model. A typical ensemble model can be seen in Fig. 5. The creation of diverse sub-models is usually performed using bagging or boosting [36], however in our case; where a variety of different panels with multiple different failures are available, we opted in using the database of the SSPs and build sub-models, for each unique SSP. This option provides not only a variety of different failure scenarios and lifetimes, but also variety of different loading conditions and initial damages.

3.2. Similarity analysis

To effectively exploit the output of the diverse sub-models an efficient dynamic-weighting strategy is implemented. Similar to [37], a Fuzzy Similarity Analysis (FSA) scheme is proposed, to calculate dynamic, time varying weights for each sub-model. More specifically, we aim to estimate the similarity between each MSP's degradation curve, as described by the Health Indicator HI_{GA}, with each SSP's from the

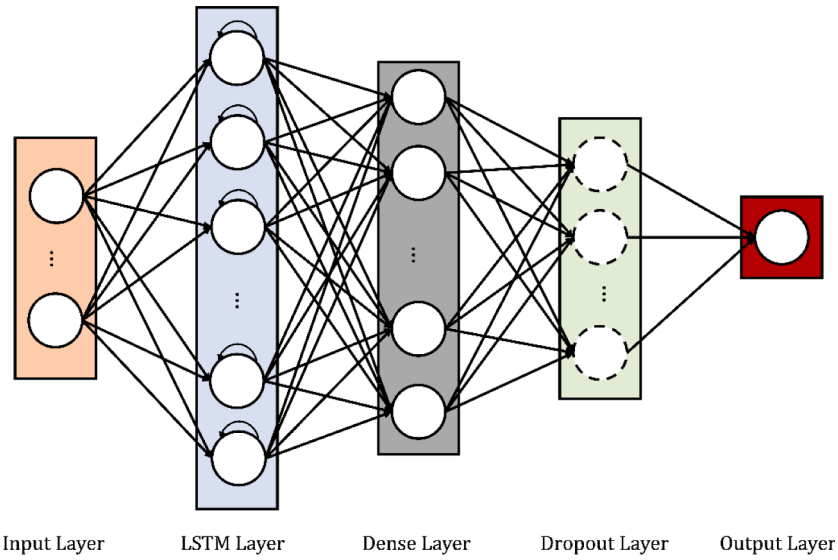

Fig. 6. Proposed LSTMN network architecture.

available historic database. In total there are $M = 15$ available degradation instances of HI_{GA} comprising our database.

Let $D = (d_1,d_2,\ldots, d_N)$ be the degradation trend of a jth SSP and $x = (x_1,x_2,\ldots, x_L)$ the degradation curve of the MSP, where $L \neq N$ the different sequence lengths. Then the weights for each sub-model are calculated as follows:

- *Pointwise Euclidean distance computation.* The first step consists of calculating the Euclidean distance between D and x denoted with the vector $\delta i \times 1 = \| D - x \|^2$ for $i = 1, \ldots, \min(N, L)$.
- *Pointwise distance scoring.* There are numerous cases where the similarity measure allows for a gradual transition between "similar" and "non-similar" as stated in [38,39]. This can be achieved by resorting to a fuzzy logic modeling paradigm in which the pointwise distance $\delta_{i \times 1}$ of D and x is mapped into a corresponding similarity value $\mu_{i \times 1}$ with respect to an "approximately zero" fuzzy set. For the definition of the latter, triangular, trapezoidal, and bell-shaped are among the most popular functions [40]. In the application illustrated in this work, the following bell-shaped function shown in Eq. (1) is used, since it provides more robust results due to its gradual smoothness:

$$\mu_{i\times 1} = \exp\left(- \left(\frac{-\ln(\alpha)}{\beta^2} \right) \delta_{i\times 1} \right) \tag{1}$$

Where α and β are parameters which define the shape of the similarity measure to the fuzzy rule set. Through trial and error, $\alpha = 5.75$ and $\beta = 0.5$ are used. To address the issue of the variable sequence lengths, the similarities of SSPs with shorter sequence lengths (shorter lifetime) are set to 0 after failure has occurred, since it is considered that they do not provide any more information towards the RUL estimation. The distance score $d_l = 1 - \mu_l$ is computed, where $l = 1, \ldots, L$.

- *Weight definition.* Finally, the weight w_l given to the jth training specimen, accounting for how similar it is to the test one, is computed by the arbitrarily chosen decreasing monotone function, which guarantees that the smaller the distance d_l the larger the impact given to the jth specimen.

$$w_l = (1 - d_l)\cdot \exp\left(-\frac{1}{\beta} d_l \right) \tag{2}$$

By repeating the previous steps for all available sub-models, the weight matrix $W_{L \times M}$ is obtained. These weights are applied in the ensemble learning paradigm to derive the final output of the ensemble model for each MSP. Given HI_{GA} of one MSP as the input vector x to the prognostic sub-models created, from each SSP, the predicted value of its RUL using the subsequent $j = 1, \ldots, M$ sub-model is represented as $\hat{y}_j = f(x)$, where $f(\cdot)$ is the regression approach.

Then, the proposed simple but efficient strategy for combining sub-model outputs is to estimate the RUL as a weighted mean of those M sub-models:

$$\hat{y} = \frac{1}{M} \sum_{j=1}^{M} w_j \cdot \hat{y}_j \tag{3}$$

The idea behind the weighting of the individual $\hat{y}_j$ is that all historical degradation patterns provide some useful information for estimating the RUL of the current degradation sequence.

4. Regression algorithms

4.1. LSTM network

The Long Short-Term Memory (LSTM) neural network, which belongs to the Recurrent Neural Network (RNN) family, was initially described in [41]. Unlike traditional RNNs, LSTM includes a memory cell that assesses whether past information is still relevant or not, preventing the vanishing or exploding gradient problem when processing long sequences. Consequently, it maintains a steady error that can be back propagated through time and layers, allowing the network to learn continuously over extended periods [42].

LSTM's fundamental principle is that its memory cell serves as a repository of state information, functioning like a conveyor belt that runs through the entire chain with only minor linear interactions. The information flows effortlessly and remains unchanged. Gates, such as the forget gate, the input gate, and the output gate, are used in LSTM to remove or add information to the cell state. These gates control the passage of information along sequences, accurately capturing long-range dependencies. While working over longer periods, the gates allow LSTM units to read, write, and remove information from memory. This feature enables the units to hold only pertinent data, while discarding irrelevant information. The lower flow controls the combination of the short-term state of the last cell (h_{t-1}) and the input of the current cell (x_t), while the upper flow updates the current cell's long-term state

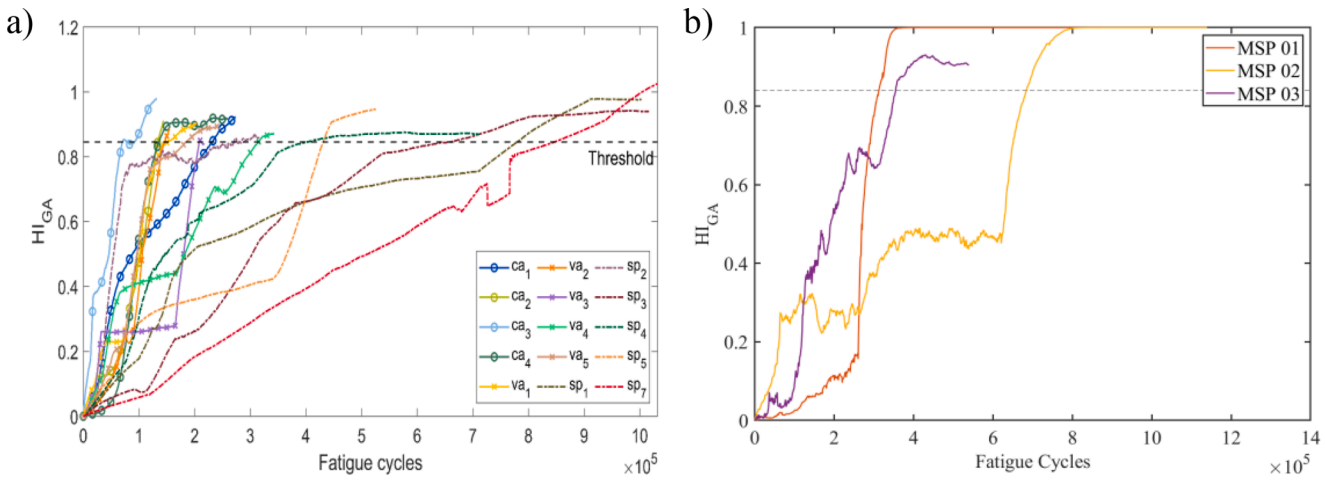

Fig. 7. HI_{GA} progression through time for the different a) SSPs and b) MSPs.

(C_t). The updating equations are

$$i_t = \sigma(W_i \cdot x_t + R_i \cdot h_{t-1} + b_i) \tag{4}$$

$$f_t = \sigma\left(W_f \cdot x_t + R_f \cdot h_{t-1} + b_f\right), \tag{5}$$

$$o_t = \sigma(W_o \cdot x_t + R_o \cdot h_{t-1} + b_0) \tag{6}$$

$$\widetilde{C}_t = \tanh(W_c \cdot x_t + R_c \cdot h_{t-1} + b_c) \tag{7}$$

$$C_t = f_t * C_{t-1} + i_t * \widetilde{C}_t \tag{8}$$

$$h_t = o_t * \tanh(C_t) \tag{9}$$

$$y_t = \sigma\left(W_y \cdot h_t + b_y\right) \tag{10}$$

The mathematical model of LSTM is shown in Eqs. (4)–(10). Where i_t, $f_t$and o_t represent the input gate, forget gate, and output gate, respectively with their appropriate weight $W_{i,f,\ o,\ c}$, $R_{i,f,\ o,\ c}$ and $b_{i,f,\ o,\ c}$ bias matrices, while the tanh, σ (sigmoid) function are the activation functions of the linear combination of $h_{t\ -\ 1}$and x_t. The gate vectors in the LSTM network serve to regulate the information flow by controlling the output value within a range of 0 to 1 [43] If the gate is set to 0, the signal is blocked. Using the equations provided above, the current state of C_t is updated based on the previous unit states $C_{t\ -\ 1}$ and the candidate cell state $\widetilde{C}_t$ which are multiplied by the forget and input gate, and then combined. Then, the o_t determines which information is converted from C_t to h_t. Lastly, as shown in Eq. (10), the output y_t is calculated according to h_t.

Our proposed LSTMN architecture can be seen in Fig. 6. The network comprises of the input layer, the LSTM layer, the fully connected layer, a dropout layer and finally, the regression output layer. The input layer accepts as input a time series data string, while dependences between input and targets are learned at the LSTM layer. Dropout layer serves as guard against overfitting and improving the generalization capabilities.

For the training of the LSTM network, since it is prone to the scale of the data, a normalization methodology is employed. The inputs and outputs need to be normalized in the desired range of [0, 1] using the minimum and maximum values of RUL from the training set, according to:

$$y' = \frac{y - y_{min}}{y_{max} - y_{min}} \tag{11}$$

Consequently, the model learns to predict the RUL in the [0, 1] range as a percentage rather than as the anticipated cycles.

Training is conducted for 100 epochs utilizing the Adam algorithm. For simplicity, the final model, which is universally used for all SSPs, has a LSTM layer with 64 hidden units, a dropout probability $p = 0.2$ and lastly the regression layer of size 1 is used to minimize the half-mean-squared-error (MSE) of the predicted responses for each time step as the loss function:

$$MSE = \frac{1}{2M}\sum_{l=1}^{M}(y_l - \hat{y}_l)^2 \tag{12}$$

M is the sequence length. For uncertainty quantification, the bootsrap algorithm [44,45] is used.

4.2. Gaussian process regression

Gaussian Processes (GP) have found extensive use in predicting the RUL of a variety of systems [46–49] and structures [13,14,19]. GPs constitute of a set of random variables following a joint Gaussian distribution, and are a function of $f(\boldsymbol{x})$ at $\boldsymbol{x}$=[x_1, x_2, …, x_n]^T. GP can be defined [50] by its mean function:

$$m(x) = E[f(x)] \tag{13}$$

And its covariance function:

$$k(x,\ x') = E[(f(x) - m(x))(f(x') - m(x'))] \tag{14}$$

Then the GP is expressed as:

$$f(x)\ \sim GP(m(x),\ k(x,\ x')) \tag{15}$$

Typically, the mean function $m(x)$ is chosen to be zero, but in our case, we opted for a linear function $m(x) = ax + b$. As noted in [50] different covariance functions yield different regression results, so the selection of this function should be done with caution based on the data. It was observed that our data are better represented by a Mattern 5/2 covariance function:

$$k(r) = \sigma_f^2\left(1 + \frac{\sqrt{5}r^2}{\sigma_l^2} + \frac{5r^2}{3\sigma_l^2}\right)\exp\left(-\frac{\sqrt{5}r}{\sigma_l}\right) \tag{16}$$

Let us consider a degradation history $H = [x_i, y_i]_{i=1}^N$, where x_i represents the input variables, and $y_i = f(x_i) + \varepsilon_i$ represents the noisy target variables, with ε_i being an i.i.d with mean 0 and variance σ_n^2 ($\varepsilon_i \sim$ *i.i.d* $N(0, \sigma_n^2)$). The joint distribution of observed target values $y = [y_i]_{i=1}^N$ and unobserved target values f^* at new input locations x^* can be denoted as:

$$\begin{bmatrix} y \\ f^* \end{bmatrix} \sim N\left(0, \begin{bmatrix} K(x,x) + \sigma_n^2 I & K(x,x^*) \\ K(x^*,x) & K(x^*,x^*) \end{bmatrix}\right) \tag{17}$$

I is the identity matrix and K a matrix containing the covariance pairs

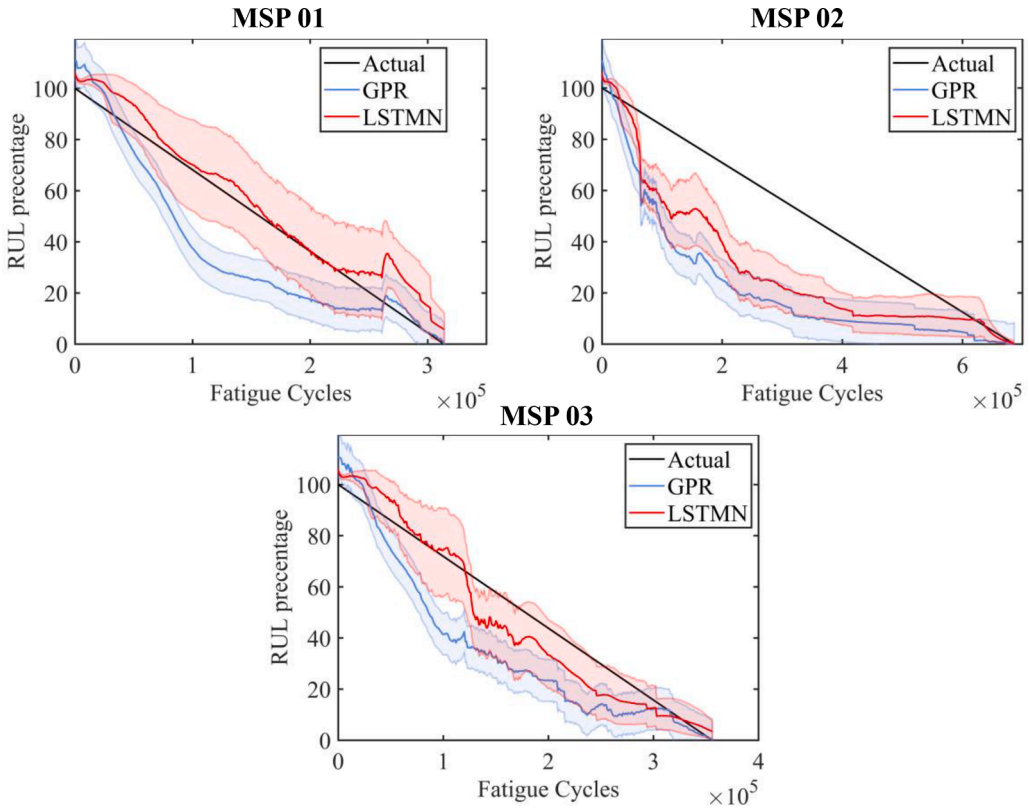

Fig. 8. RUL estimations for the different MSPs.

of$x$ and x^*. The posterior distribution for GPR, given the new inputs x^*, the historic input data x and targets y is defined by:

$$p(f^*|x,y,x^*) \sim N(\overline{f^*}, cov(f^*)) \tag{18}$$

$$\overline{f^*} = E[f^*|x,y,x^*] = K(x^*,x)\left[K(x,x)+\sigma_n^2 I\right]^{-1} y, \tag{19}$$

$$cov(f^*) = K(x^*,x^*) - K(x^*,x)\left[K(x,x)+\sigma_n^2 I\right]^{-1} K(x,x^*) \tag{20}$$

5. Results and discussion

5.1. Degradation feature

In our previous work in SSPs [29], an enhanced strain-based degradation feature was discovered using genetic algorithms. This feature denoted by HI_{GA} is presented in eq. (21). The simple HIs used to create HI_{GA} are included in the Appendix 1 for the sake of completeness.

$$HI_{GA} = vHI_1\left(HI_4 - \frac{vHI_2 + 0.5HI_3}{vHI_2}\right) + 1 \tag{21}$$

Although HI_{GA} was engineered to possess high prognosability and thus eliminate the necessity for a predefined failure threshold, the overall trend of the raw data and the scale and experimental dissimilarities between the MSPs and the SSPs required a conservative failure threshold to be set at 0.85. This value is not arbitrary and corresponds to the lowest observed value of the SSP specimens at the time of failure (see Fig. 7a) which are used to train the predictive algorithms. The progression of HI_{GA} through the lifetime for the SSPs and MSPs can be seen in Fig. 7a and b respectively. The coding of the SSPs is presented in [29] and is repeated in the Appendix. 2

It is evident, that the behavior of the HI especially at the final stages is not desirable for the two out of the three MSPs. An almost constant value of 1 is observed for several thousand cycles. This is a result of the raw strains displaying a constant value after a point as can be seen in Fig. 4b. This behavior is also intensified by vHI_1(Eq. (A.5)) which relies on the SSP data, since it needs normalization parameters [24], which are obtained through similarity analysis between the MSP and the SSPs in the first 30,000 cycles. The observed plateaus may be attributed to the impact damage stopping to propagate/ grow, and hence the strain field is no longer changing, leading to this constant behavior on both the raw strain and the HI. A second reason could be that under the same damage conditions (size, growth) the SSPs may have failed or are close to failure and this is why HI_{GA} for the MSPs is 1. The adoption of a failure threshold of 0.85 alleviates this problem, despite the fact that as damage is latent, we do not know the exact damage extent this failure threshold corresponds to.

5.2. RUL prediction

As previously discussed, an ensemble learning framework is proposed to tackle the challenging task of RUL estimation. Two distinct regression algorithms are used, LSTMN and GPR, and their predictions are compared and discussed. Both algorithms are trained using each unique SSP identified after the similarity analysis, and their predictive outputs are combined via a dynamically weighted average, as described in Prognostic Methods, which significantly enhances the prognostic performance. The predicted normalized mean RULs and the associated 90% confidence intervals (CIs) are shown in Fig. 8. It is evident that the overall RUL estimations for MSP 02 are rather conservative. More specifically, the predicted RUL underestimates the actual one, giving conservative predictions. However, it can be seen that both algorithms manage to converge to the true RUL near the EoL. For MSP 01 and MSP 03, the mean RUL estimations are closer to the true RUL and the LSTMN predictions are slightly better. However, GPR shows slightly better estimations near the EoL which are almost similar to the true RUL. As far as the CIs are concerned, for MSP 02 the CIs include the true RUL only at the very early and very late life-time stages with either algorithm. For MSP 01 and MSP 03 CIs of the LSTMN include the true RUL for most of

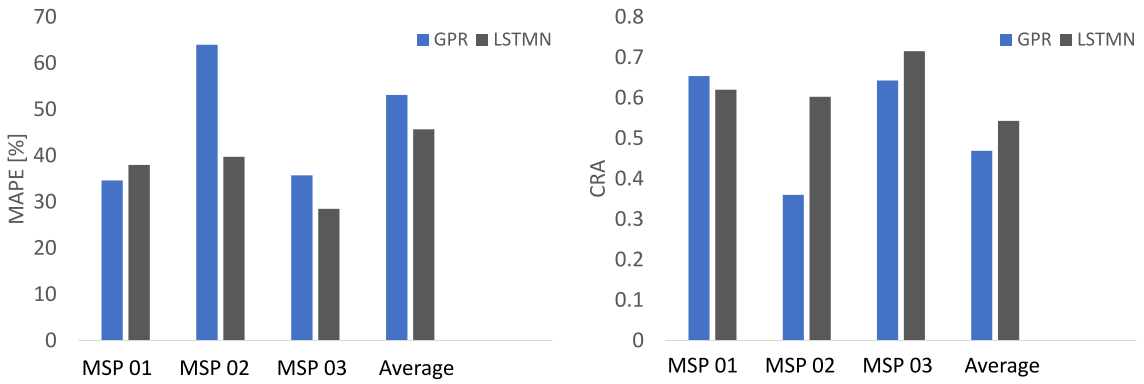

Fig. 9. MAPE and CRA for the different MSPs.

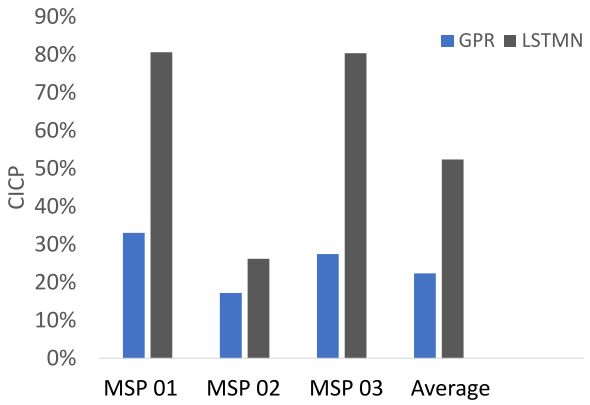

Fig. 10. CICP comparison for the different specimens and algorithms.

the lifetime, though GPR CIs only manages to include the actual RUL near the EoL.

To validate the qualitative observations regarding the RUL predictions, common prognostic performance metrics are employed [51, 52]. MAPE (Mean Absolute Percentage error) and CRA (Cumulative Relative Accuracy) are preferred (Fig. 9) since they calculate the percentage and relative differences from the true RUL and can better describe our case where the calculated RULs are in the range of [0, 1]. It can be seen, that with the exception of MSP 02, the algorithms achieve rather similar performance, with LSTM outperforming the GPR by a slight margin of less than 10%.

Regarding the CIs, CICP (Confidence Interval Coverage Probability) is employed, to measure the percentage of lifetime that is included inside the CIs. It can be seen that the bootstrap procedure followed for the LSTMN provides slightly better coverage in comparison with the GPR. More specifically, for MSP 01 and MSP 03, LSTMN's CIs include the true RUL for almost 80% of the lifetime, while GPR manages only an approximate 25%. The results are summarized in Fig. 10.

6. Conclusions

In this paper an upscaling methodology for Remaining Useful Life (RUL) estimation of multi-stiffened composite panels (MSPs) using SHM data and prognostic methodologies tested and validated only on lower hierarchically structures i.e., single-stiffened composite panels (SSPs) is presented. Unprecedented compression-compression fatigue experiments with variable amplitude are conducted on MSPs where Distributed Fiber Optical Sensors (DFOS) are employed to monitor their strain distribution along the stiffener feet. The strain data are pre-processed in two axes, the spatial and the temporal, where in the first axis a data reduction methodology is proposed while in the second an attempt to eliminate the effect of the dynamic loading is made, both trying to retain and highlight the necessary degradation information. The extracted strains are used to construct Health Indicators (HIs) proposed in previous works to monitor the structural degradation and eventually estimate the RUL. However, the behavior of the HIs near the EoL was not perfect and hence A failure threshold is set based on the data from the SSP to increase prognosability.

Regarding the RUL estimates, we treat the prognostic task as a regression one. Two standard machine learning algorithms are employed to this direction i.e., Long-Short Term Memory Networks (LSTMN) and Gaussian Process Regression (GPR). An ensemble learning similarity framework is proposed, which trains unique models using data and information from the SSP and then combines their output using a similarity-based weighted mean. More specifically, dynamic similarity is measured between the SSPs and the tested MSP and the similarity weights are used to combine the ensemble learning outputs and estimate the final RUL. Regarding confidence intervals (CIs), they are an inherent property of GPR. However, for the LSTMN, the bootsrap algorithm is used to create the CIs. The RUL estimates for the MSPs achieve a quite good performance, managing to stay close to the actual RUL especially towards the End of Life (EoL). The quality of the HI highly affects the predicted RUL and generally a more gradual HI behavior leads to better estimation of the RUL. A drawback of the proposed methodology concerns the arbitrary EoL threshold. For this threshold to be more robust and meaningful, correlation with a degradation property such as damage size or stiffness reduction is necessary and is in our intentions for future research. Overall, this first attempt of upscaling methodologies trained with SHM data in lower hierarchically structures to prognose the RUL of more complex structures is considered successful.

Though the attempt can be considered successful there are several limitations that need to be addressed. First and foremost, the methodology is data-dependent, and hence the quality of the raw data greatly affects the HIs and the results. Also, as we stated, the failure threshold is arbitrarily set, and for it to be more meaningful it is best if it is correlated with a physical property. Finally, the methodology relies on the effectiveness and reliability of the SHM system. Potential fault of the system can significantly hinder the performance and negatively affect the results.

Funding

The research work was supported by the Hellenic Foundation for Research and Innovation (H.F.R.I.) under the "First Call for H.F.R.I. Research Projects to support Faculty members and Researchers and the procurement of high-cost research equipment grant" (Project Number: 2573). A. Broer acknowledges funding from the European Union's Horizon 2020 research and innovation program (grant no.769288, ReMAP project).

Table A.1
Information for the SSPs.

Specimen #	Impact Energy/Disbond Size	Max Load	# of Cycles to failure
ca_1	10 J	−65 kN	280,098
ca_2	10	−65 kN	144,969
ca_3	10 J	−65 kN	133,281
ca_4	30 × 20 mm^2	−50 kN −60 kN *	438,000
va_1	7.4 J	−40 kN to −60 kN	202,300
va_2	10 J	−40 kN to −55 kN	243,000
va_3	10 J	−40 kN to −50 kN	217,000
va_4	25 × 20 mm^2	−35 kN to −60 kN	345,000
va_5	7.37 J	−40 kN to −60 kN	242,000
sp_1	10 J	−50.4 kN to −78.0 kN	1580,000
sp_2	10 J	−50.4 kN to −78.0 kN	529,000
sp_3	10 J	−50.4 kN to −82.0 kN	1300,000
sp_5	10 J	−45.9 kN to −78.0 kN	452,000
sp_7	25 × 20 mm^2	−45.9 kN to −59.7 kN	1160,460

Declaration of Competing Interest

The authors declare that they have no known competing financial interests or personal relationships that could have appeared to influence the work reported in this paper.

Data availability

The data that has been used is confidential.

Acknowledgements

The authors would like to acknowledge the colleagues at Delft University of technology (Aerospace Structures and Materials Laboratory and Structural Integrity and Composites group) and University of Patras (Applied Mechanics Laboratory) for the technical support and the colleagues at Smartec SA for providing the optical fibers.

Appendix 1: Health Indicators

In this appendix we list the Health Indicators that are used to create HI_{GA}. $\varepsilon^i(t)$ and ε^i_{ref} are the strain reading of sensor i at time t and reference state respectively.

Physical health indicators

$$I_1^i(t) = \frac{\left|\varepsilon^i_{ref} - \varepsilon^i(t)\right|}{\left|\varepsilon^i_{ref}\right|} \tag{A.1}$$

Evaluates the strain change at current time t relative to the reference stage (pristine or early SHM measurements)

$$HI_2^i(t) = \frac{\varepsilon^i(t)}{\frac{\sum_1^n \varepsilon^i(t)}{n}} - \frac{\varepsilon^i(t=0)}{\frac{\sum_1^n \varepsilon^i(t=0)}{n}},\ t > 0 \tag{A.2}$$

Indicates the proportion each FBG sensor contributes to the cumulative strain among the 10FBG sensors of the same foot

$$HI_3(t) = \sqrt{\sum \left(m_i HI_1^i(t)\right)^2} \tag{A.3}$$

A fusion of HI_1 for all FBG sensors, respectively, with weights being the monotonicity m_i of each HI_1^i curve

$$HI_4(t) = \sqrt{\sum \left(m_i HI_2^i(t)\right)^2} \tag{A.4}$$

A fusion of HI_2 for all FBG sensors, respectively, with weights being the monotonicity m_i of each HI_2^i curve

Virtual health indicators

$$\mathrm{vHI}_1(t) = \exp\left(-\frac{\left(d_L(t) - d_{Lmin}\right)^2}{\sigma_L}\right), \tag{A.5}$$

Where, $\sigma L = -\frac{(d_{Lmax}-d_{Lmin})^2}{2}\left[\frac{1}{\log 10\varepsilon} + \frac{1}{\log 10(\varepsilon+\delta)}\right]$

The Euclidian distance is calculated as $d_L(t) = \|Z(t) - Z_0\|$, where $Z(t)$ is the vector [$PC_1(t)$,$PC_2(t)$], where PC_1 and PC_2 are the first two principal components of a PCA The HI is normalized via a radial basis function.

$$vHI_2(t) = \sum_1^N \left(x_i(t) - x_{r_i}(t)\right)^2 \tag{A.6}$$

statistical quantity of PCA, also known as the squared sum of residual reconstructed error.

Appendix 2: Single stiffened panel information

In this appendix we present information on the panels used in our previous research (Table A.1) [29]. Three different experimental campaigns are launched, comprising of constant amplitude (ca), variable amplitude (va) and spectrum (sp) compression fatigue experiments. In ca fatigue, fatigue load is constant throughout the experiment. In va fatigue the load is applied in block of constant loads and the max load is increased if no damage growth is observed. In the sp fatigue, the fatigue sequence is generated from an algorithm and each load is randomly applied for a predefined number of cycles.

References

[1] P. Loukopoulos, et al., Reciprocating compressor prognostics of an instantaneous failure mode utilising temperature only measurements, Appl. Acoust. (2017), https://doi.org/10.1016/j.apacoust.2017.12.003.

[2] Z. Zhao, Bin Liang, X. Wang, W. Lu, Remaining useful life prediction of aircraft engine based on degradation pattern learning, Reliab. Eng. Syst. Saf. 164 (2017) 74–83, https://doi.org/10.1016/J.RESS.2017.02.007. Aug.

[3] A. Saxena, K. Goebel, C.C. Larrosa, V. Janapati, S. Roy, F.-.K. Chang, Accelerated Aging Experiments For Prognostics of Damage Growth in Composite Materials, 2011. Sep. 01Accessed: Feb. 16, 2022. [Online]. Available, https://apps.dtic.mil/sti/citations/ADA584693.

[4] J. Guo, Z. Li, M. Li, A review on prognostics methods for engineering systems, IEEE Trans. Reliab. 69 (3) (2020) 1110–1129, https://doi.org/10.1109/TR.2019.2957965. Sep.

[5] J.Z. Sikorska, M. Hodkiewicz, L. Ma, Prognostic modelling options for remaining useful life estimation by industry, Mech. Syst. Signal Process. 25 (5) (2011) 1803–1836, https://doi.org/10.1016/j.ymssp.2010.11.018.

[6] X.-.S. Si, W. Wang, C.-.H. Hu, D.-.H. Zhou, Remaining useful life estimation – a review on the statistical data driven approaches, Eur. J. Oper. Res. 213 (1) (2011) 1–14, https://doi.org/10.1016/j.ejor.2010.11.018.

[7] Y. Lei, N. Li, L. Guo, N. Li, T. Yan, J. Lin, Machinery health prognostics: a systematic review from data acquisition to RUL prediction, Mech. Syst. Signal Process. 104 (2018) 799–834.

[8] M. Chiachío, J. Chiachío, G. Rus, J.L. Beck, Predicting fatigue damage in composites: a Bayesian framework, Struct. Saf. 51 (2014) 57–68, https://doi.org/10.1016/j.strusafe.2014.06.002.

[9] T. Peng, Y. Liu, A. Saxena, K. Goebel, In-situ fatigue life prognosis for composite laminates based on stiffness degradation, Compos. Struct. 132 (2015) 155–165, https://doi.org/10.1016/j.compstruct.2015.05.006.

[10] J. Llobet, P. Maimí, J.A. Mayugo, Y. Essa, F. Martin de la Escalera, A fatigue damage and residual strength model for unidirectional carbon/epoxy composites under on-axis tension-tension loadings, Int. J. Fatigue 103 (2017) 508–515, https://doi.org/10.1016/j.ijfatigue.2017.06.026.

[11] M. Corbetta, C. Sbarufatti, M. Giglio, A. Saxena, K. Goebel, A Bayesian framework for fatigue life prediction of composite laminates under co-existing matrix cracks and delamination, Compos. Struct. 187 (2018) 58–70, https://doi.org/10.1016/J.COMPSTRUCT.2017.12.035. Mar.

[12] M. Corbetta, A. Saxena, M. Giglio, K. Goebel, Evaluation of multiple damage-mode models for prognostics of carbon fiber-reinforced polymers, in: Struct. Heal. Monit. 2015 Syst. Reliab. Verif. Implement. - Proc. 10th Int. Work. Struct. Heal. Monit. IWSHM 2015 2, 2015, pp. 609–616, https://doi.org/10.12783/SHM2015/78.

[13] Y. Liu, S. Mohanty, A. Chattopadhyay, A Gaussian process based prognostics framework for composite structures, in: Modeling, Signal Processing, and Control for Smart Structures 2009 7286, 2009, p. 72860J.

[14] Y. Liu, S. Mohanty, A. Chattopadhyay, Condition based structural health monitoring and prognosis of composite structures under uniaxial and biaxial loading, J. Nondestruct. Eval. 29 (3) (2010) 181–188, https://doi.org/10.1007/s10921-010-0076-2.

[15] N. Eleftheroglou, T. Loutas, Fatigue damage diagnostics and prognostics of composites utilizing structural health monitoring data and stochastic processes, Struct. Heal. Monit. 15 (4) (2016) 473–488.

[16] T. Loutas, N. Eleftheroglou, D. Zarouchas, A data-driven probabilistic framework towards the in-situ prognostics of fatigue life of composites based on acoustic emission data, Compos. Struct. 161 (2017) 522–529, https://doi.org/10.1016/j.compstruct.2016.10.109.

[17] N. Eleftheroglou, D. Zarouchas, R. Benedictus, An adaptive probabilistic data-driven methodology for prognosis of the fatigue life of composite structures, Compos. Struct. 245 (2020), 112386.

[18] D. Xu, P.F. Liu, Z.P. Chen, A deep learning method for damage prognostics of fiber-reinforced composite laminates using acoustic emission, Eng. Fract. Mech. 259 (2022), 108139, https://doi.org/10.1016/J.ENGFRACMECH.2021.108139. Jan.

[19] G. Galanopoulos, N. Eleftheroglou, D. Milanoski, A. Broer, D. Zarouchas, T. Loutas, An SHM data-driven methodology for the remaining useful life prognosis of aeronautical subcomponents, Lecture Notes Civil Eng. 253 (2023) 244–253, https://doi.org/10.1007/978-3-031-07254-3_24. LNCE.

[20] J. Coble, J.W. Hines, Identifying optimal prognostic parameters from data: a genetic algorithms approach, in: Annual Conference of the PHM Society 1, 2009.

[21] C. Hu, B.D. Youn, P. Wang, J. Taek Yoon, Ensemble of data-driven prognostic algorithms for robust prediction of remaining useful life, Reliab. Eng. Syst. Saf. 103 (2012) 120–135, https://doi.org/10.1016/J.RESS.2012.03.008. Jul.

[22] Y. Lei, Intelligent fault diagnosis and remaining useful life prediction of rotating machinery, in: Intell. Fault Diagnosis Remain. Useful Life Predict. Rotating Mach, 2016, pp. 1–366, https://doi.org/10.1016/C2016-0-00367-4. Oct.

[23] B.P. Duong, et al., A reliable health indicator for fault prognosis of bearings, Sensors (Switzerland) 18 (11) (2018), https://doi.org/10.3390/S18113740. Nov.

[24] G. Galanopoulos, D. Milanoski, A. Broer, D. Zarouchas, T. Loutas, Health monitoring of aerospace structures utilizing novel health indicators extracted from complex strain and acoustic emission data, Sensors 21 (17) (2021) 5701.

[25] N. Shahid, A. Ghosh, TrajecNets: Online Failure Evolution Analysis in 2D Space, United Technol. Res. Center, Penrose Wharf, Penrose Bus. Center, Cork, Irel, 2019.

[26] L. Ren, Y. Sun, J. Cui, L. Zhang, Bearing remaining useful life prediction based on deep autoencoder and deep neural networks, J. Manuf. Syst. 48 (2018) 71–77, https://doi.org/10.1016/J.JMSY.2018.04.008. Jul.

[27] P. Baraldi, G. Bonfanti, E. Zio, Differential evolution-based multi-objective optimization for the definition of a health indicator for fault diagnostics and prognostics, Mech. Syst. Signal Process. 102 (2018) 382–400.

[28] K.T.P. Nguyen, K. Medjaher, An automated health indicator construction methodology for prognostics based on multi-criteria optimization, ISA Trans. 113 (2021) 81–96, https://doi.org/10.1016/j.isatra.2020.03.017. Jul.

[29] G. Galanopoulos, N. Eleftheroglou, D. Milanoski, A. Broer, D. Zarouchas, T. Loutas, A novel strain-based health indicator for the remaining useful life estimation of degrading composite structures, Compos. Struct. 306 (2023), 116579, https://doi.org/10.1016/J.COMPSTRUCT.2022.116579. Feb.

[30] A. Broer, G. Galanopoulos, R. Benedictus, T. Loutas, D. Zarouchas, Fusion-based damage diagnostics for stiffened composite panels, Struct. Heal. Monit. (2021), 14759217211007128.

[31] M. Stein, The Phenomenon of Change in Buckle Pattern in Elastic Structures, 1959.

[32] B.G. Falzon, M. Cerini, An automated hybrid procedure for capturing mode-jumping in postbuckling composite stiffened structures, Compos. Struct. 73 (2) (2006) 186–195, https://doi.org/10.1016/J.COMPSTRUCT.2005.11.053. May.

[33] C. Li, H. Ren, Z. Zhu, C.Guedes Soares, Numerical investigation on the ultimate strength of aluminium integrally stiffened panels subjected to uniaxial compressive load, Thin-Walled Struct. 127 (2018) 221–234, https://doi.org/10.1016/J.TWS.2018.01.003. Jun.

[34] D. Inaudi, B. Glisic, Development of distributed strain and temperature sensing cables, in: 17th International Conference on Optical Fibre Sensors 5855, 2005, pp. 222–225.

[35] E. Bauer, R. Kohavi, Empirical comparison of voting classification algorithms: bagging, boosting, and variants, Mach. Learn. 36 (1) (1999) 105–139, https://doi.org/10.1023/A:1007515423169/METRICS.

[36] Y. Liu, G. Zhao, X.P.-I. Access, Deep Learning Prognostics For Lithium-Ion Battery Based On Ensembled Long Short-Term Memory Networks, ieeexplore.ieee.org, 2019. Accessed: Feb. 22, 2023. [Online]. Available, https://ieeexplore.ieee.org/abstract/document/8815721/.

[37] J. Liu, V. Vitelli, E. Zio, R. Seraoui, A novel dynamic-weighted probabilistic support vector regression-based ensemble for prognostics of time series data, IEEE Trans. Reliab. 64 (4) (2015) 1203–1213, https://doi.org/10.1109/TR.2015.2427156. Dec.

[38] E. Binaghi, A. Ventura, A. Rampini, R. Schettini, Fuzzy reasoning approach to similarity evaluation in image analysis, Int. J. Intell. Syst. 8 (7) (1993) 749–769, https://doi.org/10.1002/INT.4550080702.

[39] A. Joentgen, L. Mikenina, R. Weber, H.J. Zimmermann, Dynamic fuzzy data analysis based on similarity between functions, Fuzzy Sets Syst. 105 (1) (1999) 81–90, https://doi.org/10.1016/S0165-0114(98)00337-6. Jul.

[40] F. Di Maio, E. Zio, Failure prognostics by a data-driven similarity-based approach, Int. J. Reliab. Qual. Saf. Eng. 20 (1) (2013), https://doi.org/10.1142/S0218539313500010. Mar.

[41] S. Hochreiter, J. Schmidhuber, Long short-term memory, Neural Comput. 9 (8) (1997) 1735–1780, https://doi.org/10.1162/NECO.1997.9.8.1735. Nov.

[42] S. Bouktif, A. Fiaz, A. Ouni, M.A. Serhani, Optimal deep learning LSTM model for electric load forecasting using feature selection and genetic algorithm: comparison with machine learning approaches †, Energies 2018 11 (7) (2018) 1636, https://doi.org/10.3390/EN11071636. *Vol. 11, Page 1636*Jun.

[43] Z. Shi, A. Chehade, A dual-LSTM framework combining change point detection and remaining useful life prediction, Reliab. Eng. Syst. Saf. 205 (2021), 107257, https://doi.org/10.1016/J.RESS.2020.107257. Jan.

[44] A. Khosravi, S. Nahavandi, Comprehensive Review of Neural Network-Based Prediction Intervals and New Advances, ieeexplore.ieee.org, 2011. Accessed: Sep. 22, 2022. [Online]. Available, https://ieeexplore.ieee.org/abstract/document/5966350/.

[45] K. Li, R. Wang, H. Lei, T. Zhang, Y. Liu, X. Zheng, Interval prediction of solar power using an Improved Bootstrap method, Sol. Energy 159 (2018) 97–112, https://doi.org/10.1016/J.SOLENER.2017.10.051. Jan.

[46] K. Liu, N.Z. Gebraeel, J. Shi, H.M. Stewart, A data-level fusion model for developing composite health indices for degradation modeling and prognostic analysis the authors are with the, IEEE Trans. Autom. Sci. Eng. 10 (3) (2013), https://doi.org/10.1109/TASE.2013.2250282.

[47] M. Li, M. Sadoughi, S. Shen, C. Hu, Remaining useful life prediction of lithium-ion batteries using multi-model Gaussian process, in: 2019 IEEE Int. Conf. Progn. Heal. Manag. ICPHM 2019, 2019, https://doi.org/10.1109/ICPHM.2019.8819384. Jun.

[48] M. Benker, A. Bliznyuk, M.F. Zaeh, A Gaussian process based method for data-efficient remaining useful life estimation, IEEE Access 9 (2021) 137470–137482, https://doi.org/10.1109/ACCESS.2021.3116813.

[49] S. Roberts, M. Osborne, M. Ebden, S. Reece, N. Gibson, S. Aigrain, Gaussian Processes For Time-Series Modelling, 2013, https://doi.org/10.1098/rsta.2011.0550. Gaussian processes for time-series modelling.

[50] C.K. Williams, C.E. Rasmussen, Gaussian Processes For Machine Learning, 2, MIT press, Cambridge, MA, 2006.

[51] A. Saxena, et al., Metrics for evaluating performance of prognostic techniques, in: 2008 international conference on prognostics and health management, 2008, pp. 1–17.

[52] A. Oikonomou, N. Eleftheroglou, F. Freeman, T. Loutas, D. Zarouchas, Remaining useful life prognosis of aircraft brakes, Int. J. Progn. Heal. Manag. 13 (1) (2022), https://doi.org/10.36001/IJPHM.2022.V13I1.3072. Jan.